Earth and Planetary Science Letters, 80 (1986) 183–199
Elsevier Science Publishers B.V., Amsterdam – Printed in The Netherlands

[4]

The stagnant bottom layer of convecting magma chambers

Claude Jaupart and Geneviève Brandeis

Institut de Physique du Globe de Paris, Université Paris 7, 4, place Jussieu, 75230 Paris Cedex 05 (France)

Received February 21, 1986; revised version accepted July 17, 1986

To interpret the many observations made on igneous complexes, a detailed understanding of the structure of the bottom boundary layer is necessary because it is there that most crystallization takes place. Magma chambers are characterized by turbulent convection and cooling through all sides. Focussing on the bottom boundary layer, its evolution is determined by two competing processes: cooling through the floor which yields a stable temperature gradient, and penetration by plumes from the convecting interior. To elucidate the physics of this interaction, we have made a series of laboratory experiments in high Prandtl number fluids undergoing transient turbulent thermal convection. At the start of the experiment, an initially isothermal plane layer of viscous silicone oil is cooled through both its upper and lower boundaries. We investigate a range of Rayleigh numbers of 10^6–10^8. We show that a stagnant layer grows at the bottom of the tank. This layer is not penetrated by convective plumes and is not affected by convective mixing. We develop a theory in good agreement with the observations and show that the stagnant layer thickness scales as $Ra^{-1/6}$. The results allow a detailed model of the temperature regime prevailing at the floor. In a basaltic magma chamber, the stagnant layer reaches a thickness of several tens of meters. A closed chamber has both a well-mixed part and a stagnant part, which implies that crystallization and differentiation proceed in a complex fashion, even if there is no reinjection.

1. Introduction

A lot of interest has recently focussed on the evolution of magma reservoirs because they may provide the key to fundamental processes operating in the interior of our planet: sea-floor spreading at mid-ocean ridges [1], magmatic differentiation and volcanic activity (for a review, see [2]). There are many fossil magma chambers at the Earth's surface which allow a direct evaluation of the processes which once operated in their molten interior. Since the pioneering studies of Bowen [3], petrologists have described many large-scale structures in igneous rocks [4–9]. Among the most spectacular are the fifteen cyclic layers found by Jackson [5] in the Ultramafic Zone of the Stillwater Complex. These horizontal layers are made of the same mineral sequence of olivine-chromite-bronzite, have an average thickness of about 50 m and can be traced throughout the whole complex over distances of more than 10 km. Jackson [5] attributed them to occasional overturns of a stagnant layer lying at the chamber bottom. More recently, following Huppert and Sparks [10], Raedeke and McCallum [11] have suggested that they were in fact due to repeated injections of hot and dense magma into the chamber. This issue can be settled by a quantitative model reproducing the field observations. This requires a proper knowledge of the structure and evolution of the boundary layer lying at the bottom of magma chambers since it is there that most crystallization takes place.

To date, studies on the physics of magma chambers have taken two different directions. Some have used numerical calculations to determine the various possible regimes for convection and differentiation in high-viscosity fluids [12,13]. Others have focussed on compositional effects due to fractional crystallization and on elegant analog laboratory experiments with aqueous solutions [10,14–18]. These apply well to the turbulent interior of magma chambers, but do not represent accurately processes occurring in horizontal boundary layers where the effects of viscosity dominate. Also, they do not span a wide range of thermal regimes. This may represent a problem since the thermal regime is a critical parameter. For example, Huppert and Turner [16] have shown that crystallization at the bottom releases buoyant

0012-821X/86/$03.50

fluid which flows upward. In experiments with the same aqueous solutions, Copley et al. [19] found that such flows are suppressed when the thermal gradient is sufficiently large. For this reason, we have undertaken a detailed investigation of the thermal regime in the lower parts of a convecting chamber. We report laboratory experiments of transient thermal convection in a viscous fluid. We then discuss to what extent crystallization modifies the observed behaviour.

Repeated influxes of magma into the chamber may perturb the thermal regime. However, as discussed above, reinjection is not a continuous process and a finite length of time separates two successive influxes. We therefore study a closed chamber. From the thermal point of view, its fundamental characteristics is that it is cooled through all sides. Focussing on the bottom boundary layer, there are two competing processes: a stabilizing temperature gradient (due to cooling through the bottom boundary) and interaction with the convecting interior. To investigate this complex situation, we have made the following experiment. We start with a fluid layer which is hot and isothermal. At time $t = 0$, we lower the temperatures of both the upper and lower surfaces by a fixed amount ΔT. Convection develops from instabilities of the upper boundary layer. In a previous paper [20], we showed that a stagnant layer develops at the tank bottom. We now give a detailed account of several experiments carried out under different conditions. We then develop a simple theory and show how to scale the stagnant layer thickness.

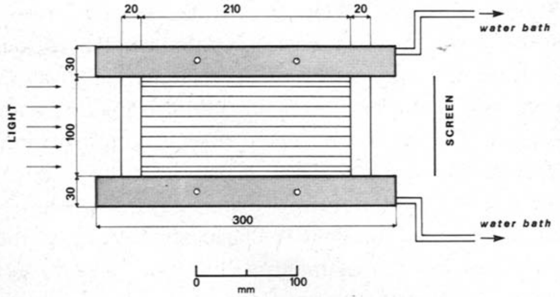

Fig. 1. Description of the experimental setup (drawn to scale with dimensions in mm). Note the 11 platinum wires stretched horizontally across the tank. Note also the finer spacing close to the upper and lower boundaries. The wires are not attached to the plexiglas walls and are free from mechanical stresses due to thermal expansion. All electrical connections and circuits are located outside the tank.

The plan of the paper is the following. In section 2, we describe the experimental setup and discuss measurement errors. Section 3 is devoted to a detailed description of the results. In section 4, we develop a theory valid for high Rayleigh numbers and compare it to the data. In section 5, we discuss the behaviour of convective plumes. We then scale our results to likely conditions in magma chambers and evaluate the general implications for the crystallization regime. The full application of our results to magmas requires the consideration of latent heat and of the kinetics of nucleation and growth [21,22], and will be postponed to a future paper for purposes of brevity. The present results are of general interest since there are very few laboratory experiments of transient convection [23–25].

2. Experimental details

2.1. General description of the apparatus

We use a plexiglas tank with 2 cm thick walls, 25 cm × 25 cm horizontal dimensions and 10 cm height (Fig. 1). The upper and lower boundaries are 3 cm thick copper plates through which thermostated water circulates. Temperature regulation is achieved through one HAAKE thermostat and one HAAKE cryostat which maintain temperature to better than 0.1°C over several days. Two thermocouples are buried in each copper plate close to the fluid in order to measure directly the boundary temperatures.

We use two kinds of visualisation techniques. First, the common shadowgraph technique which gives a picture of the whole system. Second, differential interferometry with a 4 cm diameter laser beam. Both were used to determine the structure of convection in the fluid layer [20]. The quantitative interpretation of the pictures is difficult because of light refraction effects (typical temperature contrasts exceed 10°C).

We also carry out measurements of the horizontally averaged temperature at several depths in the layer. 11 platinum wires were stretched across the tank with a spacing of 1 cm in the interior and 0.5 cm near the boundaries (Fig. 1). The wires have a diameter of 0.2 mm and do not disturb the flow significantly. They are part of an electrical circuit made of a stable precision tension generator (25 mV) and a precision resistance of 1 Ω. The tension generator is good to better than 2 μV over several days. Ohmic dissipation is totally negligible. The electrical tension across the precision resistance is measured to better than 1 μV with a 6-point Schlumberger Solartron voltmeter. This tension varies as a function of the platinum wire resistance and hence temperature. A temperature difference of 0.1°C leads to an average tension variation of 1.5 μV. Each wire is calibrated independently. Due to fluctuations in the reference tension and contact effects when switching from one wire to the next, tension variations of ±3 μV lead to uncertainties of ±0.2°C. The main problem is due to thermal expansion of the tank walls which tend to stretch the wires, thereby changing their resistance. To alleviate this, the wires are attached to soft springs which compensate for any mechanical stress. We discuss the experimental errors later.

2.2. *The experiments: procedure and parameters*

We used silicone oils manufactured by Rhone Poulenc (Table 1). The values of viscosity were measured in our laboratory with a HAAKE falling ball viscometer. The values of all the other physical properties are those given by the manufacturer.

In order to simulate conditions of instantaneous cooling, we proceeded as follows. Both copper plates were left at high temperature T_i for a time long compared to the thermal constant of the fluid layer (d^2/κ, where d is the layer thickness and κ thermal diffusivity). The fluid was thus initially isothermal. There were no detectable side-wall heat losses (no visible motions in the fluid, Fig. 2). During the same period, the cryostat was maintained in closed circuit at a much lower temperature of about 4°C. At the initial time $t = 0$, both copper plates were switched to the cryostat. After a short transient of about 3 minutes, the temperature of both copper plates dropped by about 20°C. By setting the temperature of the cryostat close to that new value, we were able to stabilize the temperature to within 0.1°C in less than 6 minutes. The difference between values of temperature at 3 minutes and in steady-state was always less than 10%. The temperature of both the upper and lower boundaries were thus maintained at a constant value T_f after 6 minutes. We always

TABLE 1

Physical properties for the silicone oils

Oil type	ρ	ν (m^2/s)	α (K^{-1})	κ (m^2/s)	Pr
47V20	0.965	2×10^{-5}	9.45×10^{-4}	1.14×10^{-7}	175
47V100	0.965	10^{-4}	9.45×10^{-4}	1.13×10^{-7}	877
47V500	0.970	5×10^{-4}	9.45×10^{-4}	1.13×10^{-7}	4425
47V1000	0.970	10^{-3}	9.45×10^{-4}	1.13×10^{-7}	8850

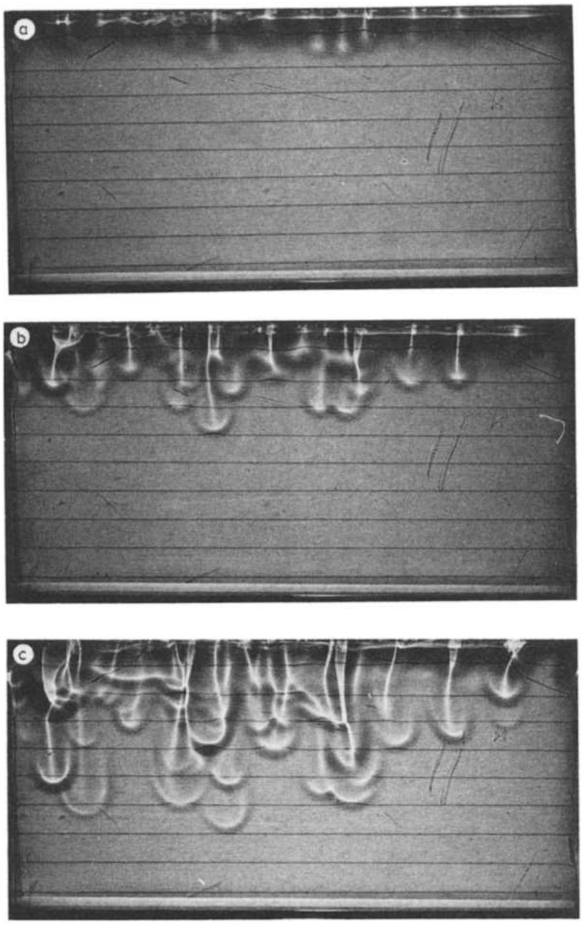

Fig. 2. Time sequence of the development of convection in experiment 1. Times are, from top to bottom: 2′, 2′7″ and 2′14″. The photographs show the whole tank. Convective instability of the upper boundary layer occurs after a finite time. Note that there is no detectable motion in the interior at the start of the experiment (top photograph). The scale is given by the wire spacing which is 1 cm.

used temperature drops of about 20°C, so that the accuracy of the temperature measurements was ±1% at the start of the experiment. The temperature contrast is $\Delta T = T_i - T_f$. These conditions approximate those of instantaneous cooling, i.e. a temperature drop ΔT at time $t = 0$.

For our experiments, the governing equations are the following in the standard Boussinesq approximation. The vertical axis 0-z is positive upwards:

$$\nabla \cdot \boldsymbol{u} = 0 \tag{1a}$$

$$\rho \frac{\mathrm{D}\boldsymbol{u}}{\mathrm{D}t} = -\nabla p + \mu \nabla^2 u + \rho \alpha T g \boldsymbol{n} \tag{1b}$$

$$\rho C_p \frac{\mathrm{D}T}{\mathrm{D}t} = k \nabla^2 T \tag{1c}$$

In these equations, $\boldsymbol{u}$ denotes velocity, $\boldsymbol{n}$ the vertical unit vector and T temperature. p is the deviation from hydrostatic pressure. ρ is the reference value of density (at T_i), α the thermal expansion coefficient, μ viscosity, C_p heat capacity and k thermal conductivity. We shall assume that all physical properties are constant. This is not exactly true for viscosity (Table 2), which varies as a function of temperature by less than 30%. The reference value of viscosity is taken at the initial temperature T_i, since we focus on the early stages of the experiment.

Using the following characteristic scales: d for spatial coordinates, d^2/κ for time, ΔT for temperature, the two parameters which characterize the experiments are the Rayleigh and Prandtl numbers:

$$Ra = \frac{g\alpha \, \Delta T d^3}{\kappa \nu} \tag{2a}$$

$$Pr = \nu / \kappa \tag{2b}$$

where ν is kinematic viscosity. We report data from nine different experiments (Table 2). Experiments were repeated in similar conditions to check the reproducibility of the results. The range of Pr investigated is 175–8850 (Table 1) which corresponds to the values for magmas [26]. The range of Rayleigh numbers is 1.6×10^6–1.8×10^8, covering two orders of magnitude. The convection regime for such high-Pr fluids can be defined according to Kraichnan [27]. It is characterized by instability of the thermal boundary layer which generates plumes (Fig. 2). Each plume first evolves in a laminar regime, with its velocity determined by the balance between viscous drag and buoyancy. The field of plumes is chaotic because of the process of plume generation. In a very thick fluid layer, each plume eventually becomes turbulent at some distance for the boundary. It then entrains surrounding fluid, which implies a change of dynamics [28]. According to Kraichnan [27], the transition to such fully developed turbulence occurs when the following condition is met:

$$Ra > 4.5 \times 10^4 \times (Pr)^{3/2} \tag{3}$$

In our experiments, this is never the case. The regime is thus one of thermal turbulence, with velocities depending on viscosity. We shall return to the plume characteristics in section 5.

TABLE 2

Parameters for the experiments

No.	Oil	T_i (°C)	T_f (°C)	ΔT (°C)	$\nu(T_i)$ (10^{-6} m^2/s)	$\nu(T_f)$	Ra_i
1	V500	54.4	32.2	22.2	312	466	5.96×10^6
2	V100	45.3	27.0	18.3	71	98	2.16×10^7
3	V100	45.5	25.7	19.8	71	101	2.35×10^7
4	V100	60.0	34.5	25.5	55	86	3.89×10^7
5	V100	31.5	19.5	12.0	91	113	1.11×10^7
6	V100	64.1	37.8	26.3	51	81	4.32×10^7
7	V1000	36.5	21.3	15.2	810	1080	1.58×10^6
8	V20	49.4	27.6	21.8	14	22	1.28×10^8
9	V20	59.4	22.9	26.5	12	23	1.83×10^8

2.3. *Temperature measurements*

We measured the resistance of each wire, which is a function of the horizontal average of temperature. The data were taken manually and then fed to a computer. We made one profile (11 readings) every 3 minutes. The average time needed for one profile was 40 seconds. From the time series for each wire, the values were smoothed with a 3-point running average and corrected for the finite time taken to make 11 readings. We thus had instantaneous profiles where all temperature measurements correspond to the same time. The measurements were usually taken for about half an hour and the system was left to come to equilibrium.

These data allow the computation of the convective heat flux. Temperature is written as:

$$T(x, y, z, t) = \overline{T}(z, t) + \theta(x, y, z, t) \tag{4}$$

where the overbar denotes the horizontal average. θ is the temperature fluctuation. Throughout the following, we drop the overbar and T denotes the horizontally averaged temperature. We assume that our data are values of T and we neglect heat losses through the vertical boundaries. Averaging the heat equation (1c) and using equation (4), the equation for the horizontally averaged temperature is (see for example [23]):

$$\rho C_p \frac{\partial T}{\partial t} = \frac{\partial}{\partial z}\left\{ k\frac{\partial T}{\partial z} - \rho C_p \overline{w\theta} \right\} \tag{5}$$

where $w\theta$ is the product of vertical velocity and temperature fluctuations. $\rho C_p \overline{w\theta}$ is the convective heat flux. In writing (1c) and (5), we have neglected the heat production term due to viscous dissipation. Equation (5) can be rearranged:

$$\frac{\partial}{\partial z}\left(\rho C_p \overline{w\theta}\right) = k\frac{\partial^2 T}{\partial z^2} - \rho C_p \frac{\partial T}{\partial t} \tag{6}$$

Integrating this equation between heights 0 and z, we get:

$$\rho C_p \overline{w\theta}(z) - \rho C_p \overline{w\theta}(0) = \int_0^z \left(k\frac{\partial^2 T}{\partial z^2} - \rho C_p \frac{\partial T}{\partial t} \right) \mathrm{d}z \tag{7a}$$

At the lower horizontal boundary, $\overline{w\theta}(0) = 0$, and (6) can be reduced to:

$$\rho C_p \overline{w\theta}(z) = k\frac{\partial T}{\partial z}(z) - k\frac{\partial T}{\partial z}(0) - \int_0^z \rho C_p \frac{\partial T}{\partial t}\, \mathrm{d}z \tag{7b}$$

Using the temperature data, we compute all derivatives using standard second-order finite-difference formulae. The integration is made using Simpson's formula.

Accurate determinations of the wires vertical coordinates are necessary. We used a calliper-square which allows measurements to 0.1 mm. The wires were found to be horizontal to better than 0.5 mm, or about ±0.2 mm. Adding all possible errors, the heat flux data are good to about 4% at the start of the experiment. At later times, the temperature difference between the fluid and the horizontal boundaries decreases, thus the accuracy on temperature and heat flux also decreases.

There are other sources of errors. One is the finite time to read all 11 temperature data. In the very early transient stages, the method applied for correction is not accurate. Another source of error is of a more fundamental nature: heat losses through side-walls. In order to minimize them, we worked at temperatures close to room temperature. Starting with a fluid hotter than ambient air, we did not notice any side-wall flows (Fig. 2). Throughout the experiment, transient heat conduction in the plexiglas walls can be neglected because it has a characteristic time of several hours, or more than the duration of the experiment. One way to look at this problem is to integrate the heat equation (5) over the whole layer. Neglecting side-wall heat losses, and using the fact that the convective heat flux is zero at horizontal boundaries, this equation yields:

$$\int_0^d \rho C_p \frac{\partial T}{\partial t}\, \mathrm{d}z = k\frac{\partial T}{\partial z}(d) - k\frac{\partial T}{\partial z}(0) \tag{8}$$

Because all terms can be computed independently from the T data, the overall error on (8) can be determined. This closure error was found to be 10–15%, corresponding to systematic underestimation of heat loss terms (RHS) compared to the enthalpy decrease term (LHS). Because it is systematic, it cannot be blamed on the temperature data. Part of it can be due to side-wall heat losses, but we attribute it to an error in the computation of the temperature gradient at the upper boundary. There, the temperature profile is very steep [29] and there are not enough data points to allow a good determination of the gradient. This implies a systematic underestimation which is of the same order as the calculated closure error. As cooling proceeds, the upper boundary layer thickens and the accuracy of the gradient estimate should improve. Indeed, we find that the closure error decreases. We conclude that the errors on heat flux are those listed above, except in the upper boundary layer. As will be seen later, we are not interested in the absolute values of convective heat flux, but rather on how it varies with depth in the well-mixed layer. We shall show results from two similar experiments which make it clear that reproducibility is better than 4%, in agreement with the error estimate.

3. General description

All experiments behave similarly as discussed in [20]. We now describe the salient features. At time $t = 0$, the temperature of both the top and bottom boundaries are lowered. After a finite length of time, the upper boundary layer goes unstable and descending plumes are generated (Fig. 2). This first instability occurs when a Rayleigh number defined locally with the thermal boundary layer thickness reaches a critical value (Appendix 1).

The plumes almost reach the tank bottom, but not quite. As shown in our previous report [20], a stagnant layer is observed to grow there. This layer is not penetrated by the downgoing plumes and is therefore isolated from the convecting interior. Using differential interferometry, we gave in this report additional visual demonstration that there is no penetration. By carrying out the reverse experiment, i.e. heating a cold layer from both top and bottom, we were further able to show that the temperature variation of viscosity plays no role in the process [20]. Initially, the stagnant layer grows very fast, and slows down as time increases (Fig. 3). We did not use the photographs to measure systematically the stagnant layer thickness because of light refraction effects. We now focus on the numerical data.

Temperature and heat flux data for two different experiments are given in Figs. 4 and 5. The reproducibility of the results is assessed in Figs. 4b and 4c. Note that heat flux values differ by less than 8% everywhere. This is partly due to the 12% contrast in Rayleigh number, and the remaining is entirely compatible with the 4% error estimate.

Several features must be noted on the temperature profiles. First, the presence of two thermal boundary layers. The top one is unstable and is the site of plume genesis. The bottom one is associated with a stable density gradient. The aim of this study is to develop a model for this layer. The second feature is that temperature is approximately uniform in the middle: this is a well-mixed layer. To the experimental error, it is not possible to detect whether the mean temperature profile is slightly stable or not there. The third feature is the transient behaviour of temperature: the fluid layer is cooling continuously.

The heat flux profiles (Figs. 4b and 5b) show two features of interest. First, heat flux decreases linearly with depth in the well-mixed layer. This is analogous to the results of Deardorff et al. [23] and easy to understand from equation (5). In the well-mixed layer, temperature is independent of z and has a value $T_m(t)$. The equation therefore reduces to:

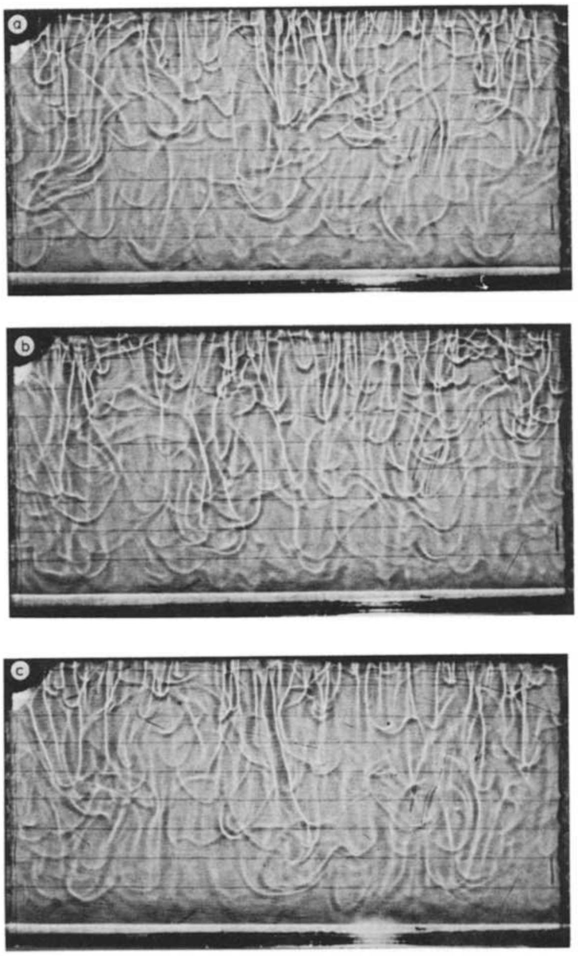

Fig. 3. Time sequence of the evolution of convection in experiment 8. Times are, from top to bottom: 3′, 4′ and 7′. A dark region is seen to grow at the bottom which is not penetrated by convective plumes. This is the stagnant layer. Due to the strong refraction of light in the boundary layers, the wire located at a height of 1 cm is seen at the very bottom of the pictures (in the white area). In the last photograph, the top of the stagnant layer is at a height of about 1.6 cm, or 0.16 in non-dimensional units.

$$\rho C_p \frac{\mathrm{d}T_m}{\mathrm{d}t} = -\frac{\partial}{\partial z}\left\{\rho C_p \overline{w\theta}\right\} \tag{9}$$

This equation shows that the vertical gradient of the convective heat flux is independent of z and is proportional to the cooling rate. The second feature is that heat flux is zero over a certain thickness at the bottom (Figs. 4b and 5b). This is consistent with the observation that convective

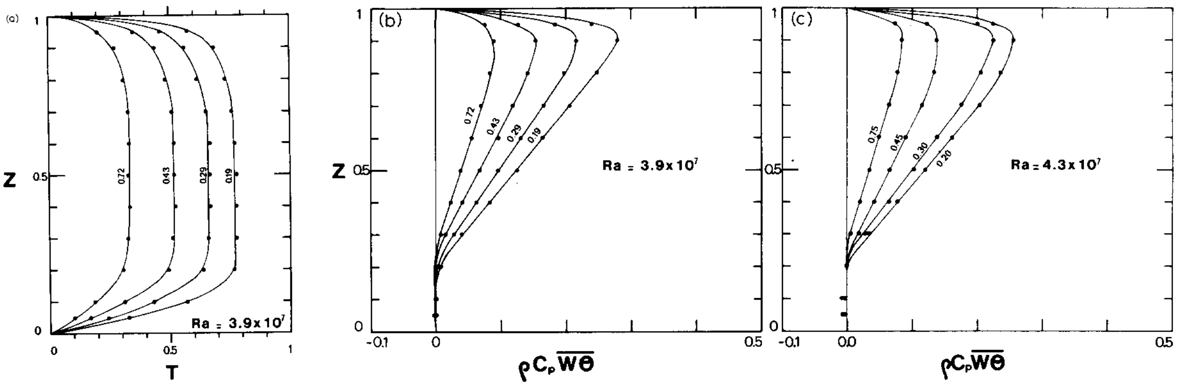

Fig. 4. (a) Vertical profiles of temperature in experiment 4. Numbers along the curves are values of non-dimensional time t^* (equation (17b)). Dots indicate the measured values. The smooth curves were drawn arbitrarily. (b) Vertical profiles of convective heat flux in the same experiment and for the same times. Convective heat flux is made dimensionless according to equation (16). Note the linear decrease in the middle of the fluid layer and the small values (not significantly different from zero) at the bottom. (c) Vertical profiles of heat flux for experiment 6 which corresponds to a similar Rayleigh number. Note the good agreement with (b).

plumes do not reach the tank bottom where a stagnant layer grows. Because of the errors in the heat flux values, it is not possible to state this as proof that there is indeed no convection in that layer. The proof was given in our previous report [20] using visualization techniques.

The errors are too large to show that heat flux is really zero in the bottom boundary layer. However, we can compare our measured values to those reported by Deardorff et al. [23] in their experiments. They showed marked penetration in a stable temperature gradient with negative heat flux values reaching ten per cent of the maximum heat flux into the layer. Such high values are ruled out by our data. The reason is of course that Deardorff et al. [23] used water where inertial effects dominate. In the viscous oils of our experiments, these are negligible and the plumes stop when they reach surroundings with the same temperature. In the lower parts of the well-mixed layer, the data suggest that heat flux departs from a linear profile and tends to zero without changing sign (Fig. 4b). This again differs from the results of Deardorff et al. [23].

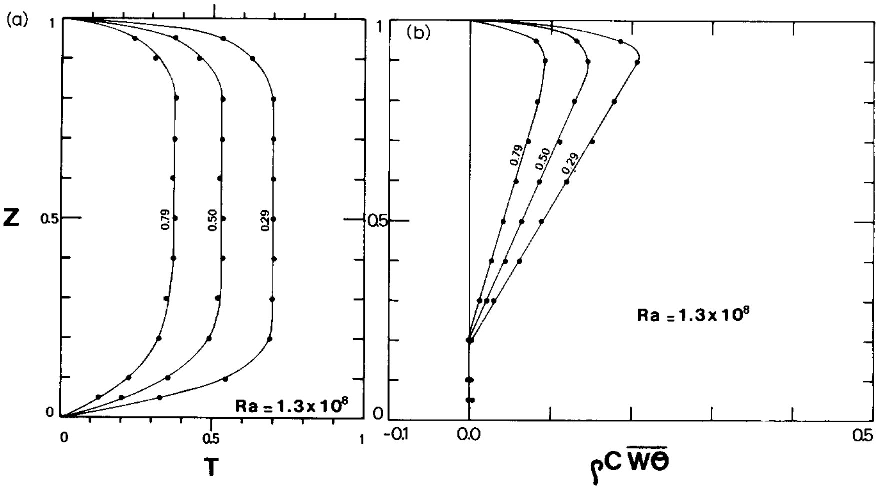

Fig. 5. (a) Vertical profiles of temperature in experiment 8. Both the upper and lower boundary layers are thinner than in experiment 4. (b) Vertical profiles of convective heat flux in the same experiment.

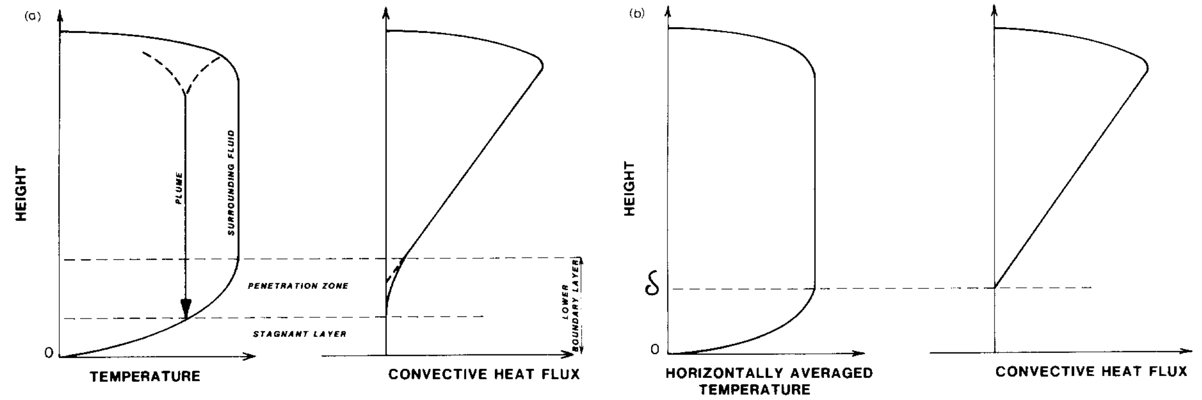

Fig. 6. (a) Schematic illustration of the basic physical aspects of the experiments. Left: cold plumes travel downwards in hotter surrounding fluid until they reach the lower boundary layer. There, they encounter fluid with colder temperature and their buoyancy decreases. They stop at the level where their temperature equals that of surrounding fluid. Right: Simplified profile of convective heat flux showing the decrease to zero in the lower boundary layer. (b) Idealized profiles for both temperature and heat flux used in theoretical considerations. The mean horizontal temperature corresponds to an average of the temperatures of plumes and surrounding fluid. The top of the stagnant layer is defined at height δ where heat flux drops linearly to zero.

From these considerations, we draw the following model for convective plumes in a high Prandtl number fluid (Fig. 6a). When they reach the stable temperature gradient, they slow down as their buoyancy decreases. They stop when they reach the level of zero buoyancy, i.e. where their temperature equals that of the surrounding fluid (Fig. 6). This level is the top of the stagnant layer. Throughout the following, we refer to an idealized model based on a simplified profile for the convective heat flux. We compute the height δ at which the linear portion of the profile intersects the vertical axis (Fig. 6b). δ is equated to the stagnant layer thickness. This provides an unambiguous definition in good agreement with the observations. For example, consider Fig. 3. The earliest computation of δ at the time of 12′, slightly later than the bottom photograph, gives 0.17, which compares well with the observed value of about 0.16.

The important point is that "stagnant" means no motion, i.e. there is no convection below height δ. Fig. 7 shows the evolution of δ as a function of time for the whole range of Rayleigh numbers investigated. Note that the stagnant layer gets thinner as the Rayleigh number increases. Note also the fast rate of growth in the beginning. We now use simple theoretical considerations to derive an expression for $\delta(t)$.

4. A simple model

4.1. The evolution of temperature

The heat equation (5) can be integrated between heights δ and d:

$$\rho C_p \int_\delta^d \frac{\partial T}{\partial t}\,\mathrm{d}z = k\left[\frac{\partial T}{\partial z}(d) - \frac{\partial T}{\partial z}(\delta)\right] - \rho C_p\{\overline{w\theta}(d) - \overline{w\theta}(\delta)\} \qquad (10)$$

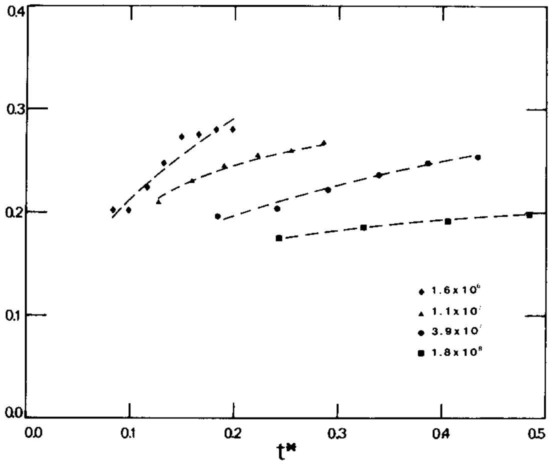

Fig. 7. Thickness of the stagnant layer versus non-dimensional time for experiments spanning the whole range of Rayleigh numbers. Note that the stagnant layer gets thinner as the Rayleigh number increases.

By definition (Fig. 6), $\partial T/\partial z(\delta) = 0$ at the edge of the well-mixed layer, and also $\overline{w\theta}(\delta) = \overline{w\theta}(d) = 0$. Hence equation (10) reduces to:

$$\int_\delta^d \frac{\partial T}{\partial t}\,\mathrm{d}z = \kappa\frac{\partial T}{\partial z}(d) \tag{11}$$

We treat the case of high Rayleigh numbers. In this limit, both the upper and lower boundary layers are of negligible thickness, hence:

$$\int_\delta^d \frac{\partial T}{\partial t}\,\mathrm{d}z \approx d\frac{\mathrm{d}T_\mathrm{m}}{\mathrm{d}t} \tag{12}$$

where T_m is the temperature in the well-mixed layer. To close the problem, we need a formula for the heat flux through the upper boundary, $Q(d) = -k\ \partial T/\partial z(d)$. Dimensional considerations led Townsend [30] and Deardorff et al. [23] to the following expression:

$$Q(d) = -k\frac{\partial T}{\partial z}(d) = -Ck\left\{\frac{g\alpha}{\kappa\nu}\right\}^{1/3} T_\mathrm{m}^{4/3} \tag{13}$$

where C is some constant. Howard [31] gave a simple physical model to justify this expression. Lower values for the (1/3) exponent have been suggested by many authors. Katsaros et al. [29] made a careful laboratory study to investigate this specific problem and concluded that the exponent was indeed 1/3, down to Rayleigh numbers of 10^6. More recently, Ho-Liu et al. [32] have used an improved method to compute heat flux in numerical calculations of convection and found a value of 0.327 for Rayleigh numbers ranging from 10^4 to 10^6. These results confirm the validity of expression (13). From their experiments, Townsend [30] and Deardorff et al. [23] found values of constant C ranging from 0.19 to 0.23. We shall take a mean value of 0.21, remembering that the error introduced by this choice is small (10%). Expression (13) will be used to make heat flux dimensionless with the following heat flux scale:

$$\overline{Q} = Ck\left\{\frac{g\alpha}{\kappa\nu}\right\}^{1/3} \Delta T^{4/3} \tag{14}$$

Using equations (12) and (13), we find:

$$\frac{\mathrm{d}T_\mathrm{m}}{\mathrm{d}t} = -C\frac{\kappa}{d}\left\{\frac{g\alpha}{\kappa\nu}\right\}^{1/3} T_\mathrm{m}^{4/3} \tag{15}$$

Throughout the following, temperature is calculated with reference to that of the two boundaries, i.e. it is initially ΔT in the interior and zero at the boundaries. Equation (15) can be made dimensionless using ΔT as temperature scale and the following time-scale:

$$\tau = \frac{3}{C}\frac{d^2}{\kappa}Ra^{-1/3} \tag{16a}$$

The dimensionless temperature and time are:

$$T_\mathrm{m}^* = T_\mathrm{m}/\Delta T \tag{16b}$$

$$t^* = t/\tau \tag{16c}$$

Equation (15) is integrated for the initial condition $T_\mathrm{m}^*(0) = 1$:

$$T_\mathrm{m}^* = (1 + t^*)^{-3} \tag{17}$$

This dimensionless function is plotted in Fig. 8a

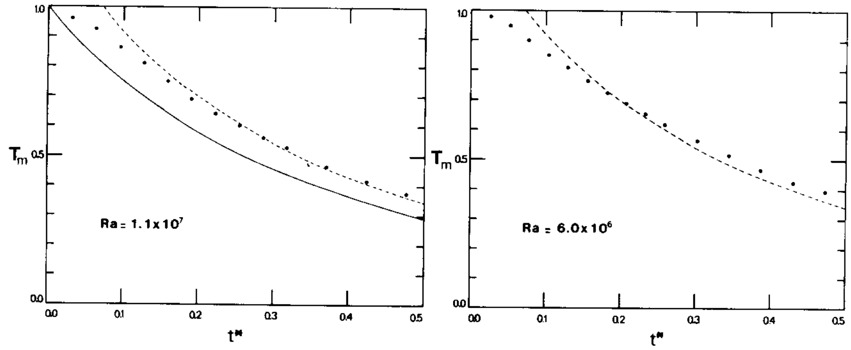

Fig. 8. Evolution of T_m, the temperature in the well-mixed layer, versus non-dimensional time t^*. (a) Experiment 5. The solid curve is theoretical estimate from equation (19). The discrepancy between the theoretical prediction and the measured value is mainly due to the non-instantaneous cooling conditions at the experiment start. The dashed curve is obtained by translating the solid curve along the time axis, which amounts to shifting the initial time. (b) Same as (a) for experiment 1. The theoretical prediction is not as good as in (a) because the Rayleigh number is smaller.

together with data from experiment 5. Rather than collapsing all data onto a single curve, we prefer to report individual cases so that each experiment can be appreciated on its own. The misfit of Fig. 8a is due to the fact that our laboratory conditions do not correspond exactly to the instantaneous conditions assumed to obtain (17). The experimental data can be superimposed onto the theoretical curve by a translation along the time-axis, i.e. changing the initial time to allow for the fact that temperature did not drop instantaneously. For comparison, the time of 6 minutes corresponds to a non-dimensional time of 0.064 for the experiment of Fig. 8a (experiment 5). It would be of course possible to integrate equation (11) with the experimental conditions, but we feel it is not worth the effort. Rather than making a theory to reproduce the data perfectly, we prefer to show that simple concepts are sufficient to understand the experiments. Fig. 8b gives an example of temperature data for a lower Rayleigh number of 6.0×10^6, for which the high *Ra* approximation is less valid.

4.2. The growth of the stagnant layer

We have shown that there is no convection below height δ (Fig. 6b). Thus, in the stagnant layer, heat transfer is by conduction only and the temperature equation is:

$$\frac{\partial T}{\partial t} = \kappa \frac{\partial^2 T}{\partial z^2} \tag{18}$$

This equation must be solved for the following initial and boundary conditions (in dimensionless form):

$$T(z, 0) = 1 \tag{19a}$$

$$T(0, t) = 0 \tag{19b}$$

$$T(\delta, t) = T_{\mathrm{m}}(t) \tag{19c}$$

$$\partial T/\partial z(\delta, t) = 0 \tag{19d}$$

$$\delta(0) = 0 \tag{19e}$$

Boundary condition (19c) states that the temperature at the edge of the stagnant layer is that of the well-mixed layer, i.e. the known function (17). Solving (18) with conditions (19) leads to a moving-boundary problem with $\delta(t)$ as unknown. Rather than going through a numerical method, we use the integral method which gives an approximate solution sufficient for our purposes. We integrate (18) over the vertical between $z = 0$ and $z = \delta$. This yields, using (19d):

$$\int_0^\delta \frac{\partial T}{\partial t}\, \mathrm{d}z = -\kappa \frac{\partial T}{\partial z}(0) \tag{20}$$

We approximate $T(z, t)$ with a second-degree polynomial with time dependent coefficients. In the case of instantaneous cooling of a half-space, the error function solution, this method has an accuracy of 3%. The profile is thus, using boundary conditions (19b, c, d):

$$T(z, t) = T_{\mathrm{m}}(t)\left\{ -\left(\frac{z}{\delta}\right)^2 + 2\left(\frac{z}{\delta}\right)\right\} \tag{21}$$

Substituting this into the integral equation (20), we get:

$$T_{\mathrm{m}}\delta \frac{\mathrm{d}\delta}{\mathrm{d}t} = 6\kappa T_{\mathrm{m}} + 2\delta^2 \frac{\mathrm{d}T_{\mathrm{m}}}{\mathrm{d}t} \tag{22}$$

This simple equation shows that the evolution of the stagnant layer depends on two competing processes. The first is conduction cooling (first term on the RHS), which tends to thicken the stagnant layer. The other process is due to the convective plumes (second term on the RHS), which tend to erode the stagnant layer. We call this process "convective erosion". If conduction dominates (small $\mathrm{d}T_{\mathrm{m}}/\mathrm{d}t$), the stagnant layer grows unhampered by what happens above. If convective erosion is strong (large $\mathrm{d}T_{\mathrm{m}}/\mathrm{d}t$), cooling yields colder plumes which reach deeper and deeper levels in the lower boundary layer, hence leading to the disappearance of the stagnant layer.

The trick of this analysis is that, at high Rayleigh numbers, the boundary layers are negligible in the overall heat budget, hence the temperature of the well-mixed layer can be determined independently of what happens in the stagnant layer. Of course, it would be possible to take into account the boundary layers in the equations and proceed in an exact fashion. The aim of this simple theory is to allow an understanding of the data and not to reproduce them exactly with a model as complex as the experiment itself.

Substituting (17) into (22), we get:

$$\left(\frac{\delta}{d}\right)^2 = \frac{12}{13}\frac{\kappa\tau}{d^2}\left\{(1+t^*) - (1+t^*)^{-12}\right\} \tag{23}$$

which can be recast as:

$$\frac{\delta}{d} = \sqrt{\frac{36}{13C}}\, Ra^{-1/6}\sqrt{(1+t^*) - (1+t^*)^{-12}} \tag{24}$$

Or, using the value of 0.21 for constant C (see above):

$$\frac{\delta}{d} = (3.63) Ra^{-1/6}\sqrt{(1+t^*) - (1+t^*)^{-12}} \tag{25}$$

The theoretical curves for several experiments at high Rayleigh numbers are reported in Fig. 9 together with measured values. For Rayleigh numbers smaller than 10^7, as shown above, the high Ra approximation is not valid. We show again the experiments separately to allow an evaluation of each case. The small misfit is again attributable to non-instantaneous cooling conditions, and shifting the time axis would lead to better agreement. To compare all our experiments, we plot the stagnant layer thickness at the dimensionless time of 0.2 against Rayleigh number (Fig. 10). We chose this particular t^* value because we had data from all experiments. Note that the agreement with the theoretical expression is good, and also that the reproducibility of the measurements is better than 5%. The data show that the stagnant layer thickness scales as $Ra^{-1/6}$.

In this analysis, the thickness of the stagnant layer depends on the shape of the temperature profile (see Fig. 6). The shape assumption determines both the multiplying factor (3.63) and the exponent (-12), but has no effect on the $Ra^{-1/6}$ dependence. To illustrate the error introduced by the shape profile, we have taken the worst possible assumption, that of a constant temperature gradient in the stagnant layer (linear temperature profile). The expression for δ then becomes:

$$\frac{\delta}{d} = (2.86) Ra^{-1/6}\sqrt{(1+t^*) - (1+t^*)^{-6}} \tag{26}$$

The difference between expressions (25) and (26) is never more than 22%. By analogy with the case of conduction cooling in a half-space, equation (25) should not be wrong by more than 3%. The agreement with our experimental data is of this order.

This theory was based on experiments with moderate Rayleigh numbers where viscosity dominates the whole flow structure [27]. However, it should hold to much higher Rayleigh numbers when eddy viscosity becomes important because it only depends on two specific assumptions: (1) the absence of inertial effects in the lower boundary layer at the bottom, and (2) equation (13) for the heat flux through the upper boundary. Both are valid at any high Rayleigh number.

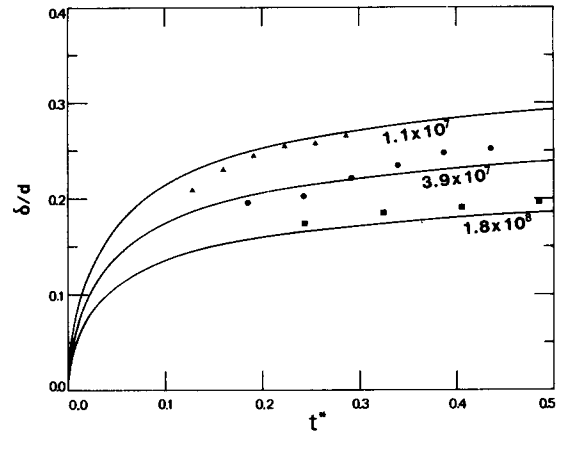

Fig. 9. Thickness of the stagnant layer versus non-dimensional time at high Rayleigh number. Solid curves are derived from theoretical equation (25).

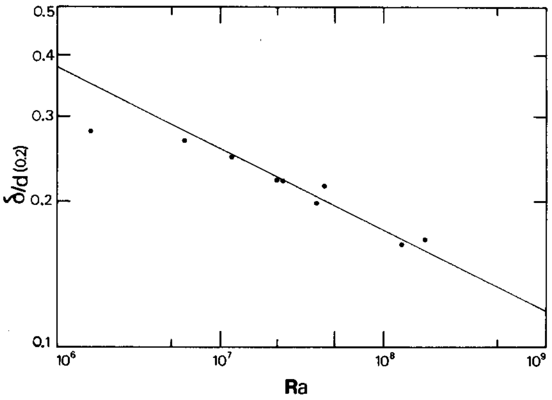

Fig. 10. Thickness of the stagnant layer at $t^* = 0.2$ for all experiments. Solid line is theoretical estimate from equation (27) and has a slope of $-1/6$. Note the good fit at Rayleigh numbers higher than 10^7. Three pairs of data at similar Ra values allow a check of the reproducibility.

5. The convective plumes

We now study in some detail the downward movement of plumes. As shown in section 2.2, all

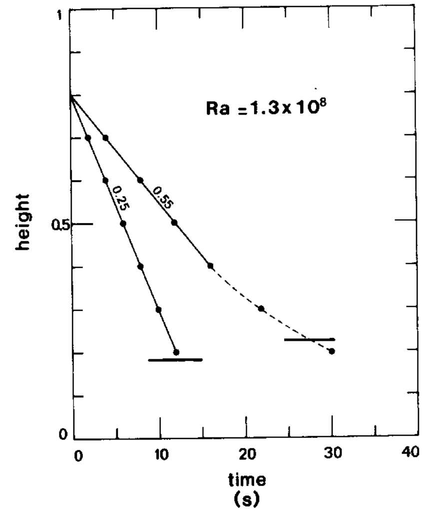

Fig. 11. Height of plume cap versus time at two stages of experiment 9 (values of the non-dimensional time are indicated along the curves). In the well-mixed layer, the curves are linear, which suggests that the plumes travel at constant velocity. The thick horizontal bars mark the edge of the stagnant layer. The plumes slow down in the lower boundary layer as they approach the stagnant layer.

our experiments are in regimes dominated by viscosity, which implies that the plumes are laminar. Looking at their fine structure (see the photographs in [20]), they are characterized by a large cap trailing a pipe, hence their dynamics must be controlled partly by those of the cap. They can be defined as laminar starting plumes, similar to those studied by Olson and Singer [33] by injecting fluid of low density into a deep layer.

We have followed their downward progression by measuring the times at which their visible tip passes each horizontal wire. Examples of such determinations are given in Fig. 11. Until they reach the lower boundary layer, they seem to move at constant velocity, contrary to an isolated turbulent starting plume [34]. Our measurements are too crude to demonstrate this fact, but independent studies support it. There are two factors of importance when assessing the behaviour of these plumes. First, they entrain little surrounding fluid. Shlien [35,36] made very careful experiments on isolated laminar starting plumes by heating a deep layer of fluid at a constant rate and found that they travel at a constant velocity. The second factor is that the plumes are not isolated and interact with neighbouring ones. Their dynamics are different since for example they cannot grow freely. Indeed, we observed that the cap does not grow noticeably during descent. Farmer [37] reported that plumes travel at a constant velocity in a lake heated by solar radiation beneath an ice cover.

From our data, it is clear that the plumes become slower as cooling proceeds, i.e. as the temperature difference across the upper boundary layer decreases (Fig. 11). This evolution parallels that of the convective velocity scale defined as follows [27]:

$$w_* = \kappa \left\{ \frac{g\alpha T_m}{\kappa\nu} \right\}^{1/3} \tag{27}$$

For each determination of plume velocity, we computed w_* using the measured values of T_m and ν at the same time. The data suggest that the plume velocity scales with w_* (Fig. 12) and yield the following result:

$$w = (5.6 \pm 0.9) w_* \tag{28}$$

This represents a standard deviation of 16%. Considering the spread of available data, from about 0.5 to 3 (Fig. 12), this result cannot be considered as experimental proof that the scaling is correct. At any given time, all plumes do not have exactly the same size, and this dispersion is responsible for a lot of scatter. Looking at the data in greater detail, we found a systematic decrease of ratio w/w_* during the course of an experiment. We attribute this to the "crowding" effect in a field of plumes. At the start of the experiment, the upper

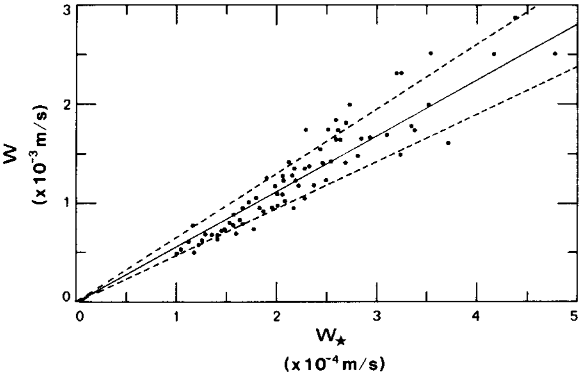

Fig. 12. Plume velocity versus velocity scale w_* (equation (29)). The solid and dashed lines correspond to relationship $w/w_* = 5.6 \pm 0.9$.

boundary layer is thin and the plumes are numerous. At the end, convection is sluggish and few plumes are seen. Thus, the dynamics of mutual interaction are changed. Selecting data from only the first few minutes of the experiments would provide a better relationship than (28), but at the expense of fewer data.

6. Implications for basaltic magma chambers

The experiments were made with the simplest thermal conditions to limit the number of parameters and for purposes of clarity. They were designed to show how penetration occurs in viscous fluids and how temperatures can be calculated at the bottom of a convecting chamber. The analysis of section 4.2 can be generalized to various cases. We now review the implications for crystallization in a basaltic magma chamber. We first discuss the values for the various variables of importance and then evaluate the effects of fractional crystallization.

6.1. The stagnant layer in a basaltic magma chamber

To apply the results to a true magma chamber, one must specify the boundary conditions at the top and bottom, which breaks down into two problems. One is that the initial temperature contrasts at the roof and floor are probably not equal, with a higher value at the roof because country rocks are colder there. The other is that the boundary condition at the roof is probably closer to one of constant heat flux, since heat flow is limited in country rocks of finite conductivity and permeability. A related problem is the lack of knowledge of the initial magma temperature upon intrusion. These preclude the determination of the Rayleigh number. It is commonly assumed to be very large, with values in excess of 10^{12} [16]. However, Marsh [38] has argued that its maximum value must be about 10^7 because of the heat flow value through country rocks. We note that even an error of several orders of magnitude has a small effect on the stagnant layer thickness which scales as $Ra^{-1/6}$.

These difficulties are not limiting and it is possible to describe in a simple and general way the conditions prevailing at the floor of a magma chamber. For small times t^*, less than 0.1, say, convection can be neglected and the problem is reduced to one of pure conduction cooling in a half-space. In other words, the solution depends only on local conditions, without any influence from those at the other boundaries and in the interior. We shall see that such small times allow crystallization over a thickness which is comparable to that of igneous layering. The stagnant layer evolution is determined by the two competing processes defined in equation (22). For small times, the layer grows freely because the process of convective erosion is negligible. At later times, this process becomes important and impedes the layer growth. Its intensity depends on the difference between the temperature contrasts at the roof and floor. In the likely case where the contrast is smaller at the floor, convective erosion would be stronger than in our experiments. The stagnant layer would grow at the same rate initially and more slowly later. It could even get thinned progressively if convective erosion is particularly strong. We emphasize that convective erosion acts over the characteristic time τ, which is large, and hence that the stagnant layer exists for a long time.

Because of these difficulties, we cannot compare our results to field conditions in detail. Nevertheless, it is instructive to have in mind the magnitudes reached by the variables in a basaltic magma chamber. Values for the relevant parameters are listed in Table 3. The magma viscosity is 10^2 Pa s, which is in the upper range for basalts [26], and the temperature difference is 100°C. The chamber thickness is 5 km. For this set of parameters, the Rayleigh number is 2.5×10^{17}, and the characteristic time τ (equation 16a) is 8.1×10^8 s, or about 26 years. The stagnant layer reaches a thickness of 33 m by time τ (Fig. 13a). Fig. 13b shows that the bottom heat flux remains large

TABLE 3

Parameters for a basaltic magma chamber

Parameter	Symbol	Value
Chamber thickness	d	5 km
Thermal expansion coefficient	α	5×10^{-5}
Viscosity	μ	10^2 Pa s
Density	ρ	2.8×10^3 kg/m^3
Temperature contrast	ΔT	100°C
Thermal diffusivity	κ	7×10^{-7} m^2/s

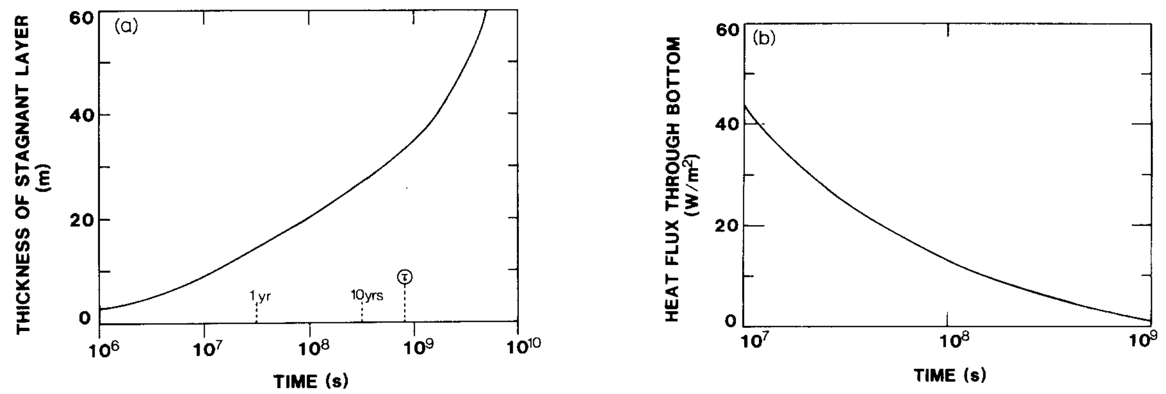

Fig. 13. (a) Thickness of the stagnant layer versus time for the set of parameters given in Table 3. This case should be close to that of a basaltic magma chamber. (b) Heat flux through the bottom boundary versus time for the same case. Note that values remain large by geological standards: more than 1 W/m^2 over the characteristic time τ.

with values of several W/m^2 throughout. At time τ, according to the calculations of Brandeis et al. [21], the floor crystallization sequence would reach a thickness of several tens of metres. As argued above, all these numerical estimates depend weakly on the assumptions. For example, at the dimensionless time of 0.1, when convective erosion is negligible, the thickness of the stagnant layer is already 18 m and crystallization has developed over about 10 m. These values depend solely on local cooling conditions and their order of magnitude is inescapable. In later times, convective erosion becomes important, but the evolution is slow.

In this quantitative analysis, all parameters do not have the same importance. For example, equation (16a) shows that the characteristic time for convective cooling τ depends weakly on both magma viscosity and temperature contrast, but that it is proportional to the chamber thickness. This implies that, regardless of uncertainties in the parameters and in the exact convective regime, the very large Stillwater magma chamber (10 km thick) cooled slowly and had a stagnant layer for a significant length of time. Here, "significant" means allowing crystallization over more than a few tens of meters.

6.2. *Implications for crystallization*

Most crystallization occurs at the floor in a region which moves inwards at a rate controlled in part by the crystallization kinetics and in part by the thermal regime [21,39]. In this region, the presence of crystals changes the viscosity [40]. However, crystallization requires undercooling and thus develops mostly in the lower parts of the stagnant layer. This implies that the characteristics of penetration are not affected. Crystallization introduces other effects. The most important is probably that it determines the effective temperature difference which drives convection [22]. For basaltic magma, Brandeis and Jaupart [22] have shown that it cannot exceed about 100°C.

To determine the complications introduced by crystallization would involve many effects: latent heat release, the kinetics of nucleation and crystal growth and fractional crystallization. These are outside the scope of the present study and we restrict ourselves to general statements. At the chamber bottom, the growth of the thermal boundary layer is impeded by convective erosion. A large temperature gradient is therefore maintained, which has implications for the crystallization regime [21]. Part of the magma is stagnant and isolated from the rest, which has implications for the development of compositional instability.

The fractional crystallization of most basaltic liquids results in the formation of light residual liquid [10,41] which is unstable and leads to "compositional convection". The density contrast due to composition usually outweighs that due to temperature, which has led many workers to neglect the thermal aspect of the problem. However, for crystallization to occur, there must be cooling and it is clear that the importance of compositional effects depends directly on the rate of crystallization and hence on the cooling rate. Further, it must be stressed that even a large density difference does not lead to instability if it exists over too small a thickness. Consider the experiments by Copley et al. [19] on the ammonium-chloride-water system. They are similar to those by Huppert and Turner [16] but focus on early stages of crystallization. The experimental set-up is that of a base-chill, i.e. a quiescent solution is cooled through the bottom only. Copley et al. [19] observed that compositional instability does not start until some time, i.e. until crystallization has been achieved over a critical thickness. Sample and Hellawell [42] have shown that this thickness corresponds to the position at which the rate of advance of the crystallization front has declined to a critical value. This value depends on the thermal regime at the bottom. The results of this paper represent a first step towards a complete analysis applicable to a convecting reservoir.

An important point is that Sample and Hellawell [42] have demonstrated that compositional instability develops out of the chemical boundary layer which lies at the top of the moving crystallization front. In their experiments, this chemical boundary layer is able to grow by chemical diffusion because the solution is quiescent. Although magma chambers are undergoing turbulent convection, we have shown that their bottom is stagnant. This means that the basic physical situation is the same and that the same mechanism for compositional instability can operate. The problem is to determine the time needed to induce it.

We conclude that compositional convection does not operate throughout the evolution of a magma chamber and that careful analysis is required to determine when it starts and at which level in the crystallization sequence its effects are felt. A final remark is that each cyclic layer of the Stillwater Ultramafic Zone extends over a few tens of meters, which is close to the stagnant layer thickness. In a chamber which was about 10 km thick [4,5], cyclic layering is therefore a small-scale phenomenon. Given the complex structure of a closed chamber which has both a well-mixed part and a stagnant part, it may be premature to attribute cyclic layering to periodic reinjections. It could be due to peculiar characteristics of crystallization in the stagnant layer. These characteristics cannot be reproduced in aqueous solutions since there can be no stagnant layer: convective plumes would penetrate deep into the stable temperature gradient, as shown by Deardorff et al. [23]. This difference reflects the role of viscosity and raises the problem of whether magmas and aqueous solutions can be treated as dynamically equivalent.

7. Conclusion

We have investigated transient thermal convection in a horizontal layer of viscous fluid cooled from both its upper and lower boundaries. We have shown that a stagnant layer develops at the bottom of the tank. This layer is not penetrated by the convective plumes coming from the top and is thus isolated from the convecting part of the layer. Simple theoretical considerations account for the experimental data. The thickness of the stagnant layer scales as $Ra^{-1/6}$, where Ra is a Rayleigh number.

The aim of this paper was to study the simplest case of transient thermal convection of relevance to magma chambers. Under such conditions, the closed system includes both a well-mixed part and a stagnant part. This structure implies that magmatic crystallization and differentiation proceed in a complex fashion, even if there is no reinjection.

Acknowledgements

We thank Claude Allègre for advice and discussions on magma chambers. Herbert Huppert, Ross Kerr, Alexander McBirney, Stephen Sparks and Stephen Tait shared many thoughts, and Pierre Bergé gave useful hints on convection phenomena. Critical reviews by Yan Bottinga and Frank Spera led to improvements. This work was supported by ATP Dynamique des Fluides (CNRS).

Appendix 1—The onset of convective instability in the upper boundary layer

The onset of convection is not instantaneous (Fig. 2). According to Howard [31], the critical time is such that a Rayleigh number defined locally in the thermal boundary layer reaches a critical value:

$$Ra_l = \frac{g\alpha\,\Delta T\{e(t_c)\}^3}{\kappa\nu} = Ra_c \tag{A-1}$$

where $e(t_c)$ is the boundary layer thickness at the critical time t_c. In previous studies, Howard [31] and Sparrow et al. [43] referred to instantaneous cooling conditions where $e(t_c)$ is given by:

$$e(t_c) = \sqrt{\pi\kappa t_c} \tag{A-2}$$

We did not achieve instantaneous cooling conditions. The temperature profile in the fluid was therefore not given by the error function solution explicitly used to derive (A-2). Instability usually occurred at a time when the surface temperature was still decreasing. For simplicity, suppose that this decrease follows a $t^{1/2}$ law. This corresponds to a constant heat flux and has the essential features of the observed evolution: sharp decrease followed by slow convergence towards steady-state. The temperature profile next to the surface at the critical time is thus given by [44, p. 63]:

$$T(x, t_c) = \Delta T\left\{1 - \sqrt{\pi}\cdot \mathrm{ierfc}\left[x/2\sqrt{\kappa t_c}\right]\right\} \tag{A-3}$$

where x is the distance to the surface. ΔT is the temperature difference between the surface and the interior at time t_c. Note that it may not be equal to the final temperature difference. Using the same definition for the thermal boundary layer thickness as in (A-2), i.e.:

$$e(t) = \frac{\Delta T}{\partial T/\partial x(0)} \tag{A-4}$$

We obtain for the profile given by (A-3):

$$e(t_c) = 2\sqrt{\frac{\kappa t_c}{\pi}} \tag{A-5}$$

This is smaller than (A-2), which shows that the local Rayleigh number must be defined with care. In fact, for the conditions used to derive (A-5), the upper boundary condition is one of constant heat flux, and it is more rigorous to define the Rayleigh number in terms of the heat flux Q rather than the temperature contrast ΔT:

$$Q = -k\frac{\partial T}{\partial x}(0) \tag{A-6a}$$

$$Ra_l = \frac{g\alpha Q\{e(t_c)\}^4}{\kappa\nu k} \tag{A-6b}$$

Because of the way $e(t_c)$ is defined (equation (A-4)), the two definitions for the Rayleigh number (A-1) and (A-6b) are equivalent. However, the change in boundary condition implies a change of critical value [45]. In experiment 1 (Fig. 2), the critical time is 2′ and the corresponding temperature contrast is about 20°C. Using (A-5), we find that Ra_c is 433. Using (A-2), it is 1680. The first value is the correct one, close to theoretical estimates for constant heat flux boundary conditions [45].

References

1 C.R.B. Lister, On the intermittency and crystallization mechanisms of sub-sea floor magma chambers, Geophys. J.R. Astron. Soc. 73, 351–365, 1983.

2 A.R. McBirney, Igneous Petrology, 504 pp., Freeman Cooper & Co., San Francisco, Calif., 1984.

3 N.L. Bowen, The Evolution of Igneous Rocks, 332 pp., Princeton University Press, Princeton, N.J., 1928.

4 H.H. Hess, Stillwater igneous complex, Geol. Soc. Am. Mem. 80, 230 pp., 1960.

5 E.D. Jackson, Primary textures and mineral associations in the Ultramafic Zone of the Stillwater Complex, Montana, U.S. Geol. Surv. Prof. Pap. 358, 106 pp., 1961.

6 L.R. Wager and G.M. Brown, Layered Igneous Rocks, 588 pp., Oliver & Boyd, Edinburgh, 1967.

7 S.A. Morse, The Kiglapait layered intrusion, Labrador, Geol. Soc. Am. Mem. 112, 1969.

8 A.R. McBirney and R.M. Noyes, Crystallization and layering of the Skaergaard intrusion, J. Petrol. 20, 487–554, 1979.

9 T.N. Irvine, Terminology for layered intrusions, J. Petrol. 23, 127–162, 1982.

10 H.E. Huppert and R.S.J. Sparks, The fluid dynamics of a basaltic magma chamber replenished by influx of hot, dense ultrabasic magma, Contrib. Mineral. Petrol. 75, 279–289, 1980.

11 L.D. Raedeke and I.S. McCallum, Investigations of the Stillwater complex, II. Petrology and petrogenesis of the Ultramafic series, J. Petrol. 25, 395–420, 1984.

12 F.J. Spera, D.A. Yuen and D.V. Kemp, Mass transfer along vertical walls in magma chambers and marginal upwelling, Nature 310, 764–767, 1984.

13 F.J. Spera, D.A. Yuen, S. Clark and H.J. Hong, Double diffusive convection in magma chambers: single or multiple layers?, Geophys. Res. Lett. 13, 153–156, 1986.

14 C.F. Chen and J.S. Turner, Crystallization in double diffusive systems, J. Geophys. Res. 85, 2573–2593, 1980.

15 J.S. Turner, A fluid dynamical model of differentiation and layering in magma chambers, Nature 285, 313–215, 1980.

16 H.E. Huppert and J.S. Turner, A laboratory model of replenished magma chamber, Earth Planet. Sci. Lett. 54, 144–152, 1981.

17 S.R. Tait, H.E. Huppert and R.S.J. Sparks, The role of compositional convection in the formation of adcumulate rocks, Lithos 17, 139–146, 1984.

18 R.C. Kerr and S.R. Tait, Convective exchange between pore fluid and an overlying reservoir of denser fluid: a post-cumulus process in layered intrusions, Earth Planet. Sci. Lett. 75, 147–156, 1985.

19 S.M. Copley, A.F. Giamei, S.M. Johnson and M.F. Hornbecker, The origin of freckles in unidirectionally solidified castings, Metall. Trans. 1, 2193–2204, 1970.

20 C. Jaupart, G. Brandeis and C.J. Allègre, Stagnant layers at the bottom of convecting magma chambers, Nature 308, 535–538, 1984.

21 G. Brandeis, C. Jaupart and C.J. Allègre, Nucleation, crystal growth and the thermal regime of cooling magmas, J. Geophys. Res. 89, 10161–10177, 1984.

22 G. Brandeis and C. Jaupart, On the interaction between convection and crystallization in cooling magma chambers, Earth Planet. Sci. Lett. 77, 145–161, 1986.

23 J.W. Deardorff, G.E. Willis and D.K. Lilly, Laboratory experiments of non-steady penetrative convection, J. Fluid Mech. 35, 7–31, 1969.

24 F.A. Kulacki and M.E. Nagle, Natural convection in a horizontal fluid layer with volumetric heat sources, ASME J. Heat Transfer 97, 204–211, 1975.

25 F.A. Kulacki and A.A. Emara, Steady and transient convection in a fluid layer with uniform volumetric heat sources, J. Fluid Mech. 83, 375–395, 1977.

26 T. Murase and A.R. McBirney, Properties of some common igneous rocks and their melts at high temperatures, Geol. Soc. Am. Bull. 84, 3563–3592, 1973.

27 R.H. Kraichnan, Turbulent thermal convection at arbitrary Prandtl number, Phys. Fluids 5, 1374–1389, 1962.

28 J.S. Turner, Buoyancy Effects in Fluids, Cambridge University Press, Cambridge, 1973.

29 K.B. Katsaros, W.T. Liu, J.A. Businger and J.E. Tillman, Heat transport and thermal structure in the interfacial boundary layer in an open tank of water in turbulent free convection, J. Fluid Mech. 83, 311–335, 1977.

30 A.A. Townsend, Natural convection in water over an ice surface, Q. J. R. Meteorol. Soc. 90, 248–259, 1964.

31 L.N. Howard, Convection at high Rayleigh number, in: Proc. 11th Int. Cong. Applied Mechanics, H. Gortler, ed., pp. 1109–1115, Springer Verlag, Berlin, 1966.

32 P. Ho-Liu, B.H. Hager and A. Raefsky, An improved method for computing heat flux in convection calculations, EOS Trans. Am. Geophys. Union 66, 1070, 1985.

33 P. Olson and H. Singer, Creeping plumes, J. Fluid Mech. 158, 511–531, 1985.

34 J.S. Turner, The starting plume in neutral surroundings, J. Fluid Mech. 13, 356–368, 1964.

35 D.J. Shlien, Some laminar thermal and plume experiments, Phys. Fluids 19, 1089–1098, 1976.

36 D.J. Shlien, Relations between point sources buoyant convection phenomena, Phys. Fluids 22, 227–228, 1979.

37 D.M. Farmer, Penetrative convection in the absence of mean shear, Q. J. R. Meteorol. Soc. 101, 869–891, 1975.

38 B.D. Marsh, Convective regime of crystallizing magma, Trans. Geol. Soc. Am., 1985.

39 G. Brandeis and C. Jaupart, The kinetics of nucleation and crystal growth and scaling laws for magmatic crystallization, submitted to Contrib. Mineral. Petrol., 1986.

40 H.R. Shaw, T.L. Wright, D.L. Peck and R. Okamura, The viscosity of basaltic magma: an analysis of field measurements in Makaopuhi lava lake, Hawaii, Am. J. Sci. 266, 225–264, 1968.

41 R.S.J. Sparks and H.E. Huppert, Density changes during the fractional crystallization of basaltic magmas: fluid dynamic implications, Contrib. Mineral. Petrol. 85, 300–309, 1984.

42 A.K. Sample and A. Hellawell, The mechanisms of formation and prevention of channel segregation during alloy solidification, Metall. Trans. 15A, 2163–2173, 1984.

43 E.M. Sparrow, R.B. Husar and R.J. Goldstein, Observations and other characteristics of thermals, J. Fluid Mech. 41, 793–800, 1970.

44 H.S. Carslaw and J.C. Jaeger, Conduction of Heat in Solids, 510 pp., Oxford University Press, Oxford, 1959.

45 D.T.J. Hurle, E. Jakeman and E.R. Pike, On the solution of the Benard problem with boundaries of finite conductivity, Proc. R. Soc. London, Ser. A 269, 469–475, 1967.